Neurobiology of Disease

Preclinical Retinal Neurodegeneration in a Model of Multiple Sclerosis

Richard Fairless,[1,3]* Sarah K. Williams,[1,3]* Dorit B. Hoffmann,[1] Aleksandar Stojic,[1,3] Sonja Hochmeister,[4] Frank Schmitz,[2] Maria K. Storch,[4] and Ricarda Diem[1,3]

Departments of [1]Neurology and [2]Anatomy and Cell Biology, University of the Saarland, 66421 Homburg/Saar, Germany, [3]Department of Neuro-Oncology, University Clinic Heidelberg, 69120 Heidelberg, Germany, and [4]Department of Neurology, Medical University of Graz, 8010 Graz, Austria

Neurodegeneration plays a major role in multiple sclerosis (MS), in which it is thought to be the main determinant of permanent disability. However, the relationship between the immune response and the onset of neurodegeneration is still a matter of debate. Moreover, recent findings in MS patients raised the question of whether primary neurodegenerative changes can occur in the retina independent of optic nerve inflammation. Using a rat model of MS that frequently leads to optic neuritis, we have investigated the interconnection between neurodegenerative and inflammatory changes in the retina and the optic nerves with special focus on preclinical disease stages. We report that, before manifestation of optic neuritis, characterized by inflammatory infiltration and demyelination of the optic nerve, degeneration of retinal ganglion cell bodies had already begun and ultrastructural signs of axon degeneration could be detected. In addition, we observed an early activation of resident microglia in the retina. In the optic nerve, the highest density of activated microglia was found within the optic nerve head. In parallel, localized breakdown in the integrity of the blood–retinal barrier and aberrations in the organization of the blood–brain barrier marker aquaporin-4 in the optic nerves were observed during the preclinical phase, before onset of optic neuritis. From these findings, we conclude that early and subtle inflammatory changes in the retina and/or the optic nerve head reminiscent of those suggested for preclinical MS lesions may initiate the process of neurodegeneration in the retina before major histopathological signs of MS become manifest.

Introduction

Traditionally, neurodegeneration in multiple sclerosis (MS) is viewed as a secondary component, with inflammation-induced demyelination being its driving force (Ferguson et al., 1997; Trapp et al., 1998). Recently, findings from optical coherence tomography in MS patients have initiated a discussion about primary neurodegeneration occurring in the myelin-deficient retina independent of optic nerve pathology (Brandt et al., 2011; Saidha et al., 2011). Additionally, a postmortem study of MS cases reported extensive neurodegeneration of the ganglion and inner nuclear cell layers of the retina and inflammatory changes in the retina itself (Green et al., 2010), although the mechanisms underlying this pathology remain unresolved.

In general, the relationship between inflammation and neurodegeneration in MS is not fully understood, particularly with respect to the timing of onset of neurodegeneration. For example, neurodegeneration has been observed in normal-appearing white matter (NAWM) and in chronic inactive lesions (Kornek et al., 2000), suggesting that it may occur in areas with low inflammatory activity. However, in early or preactive/predemyelinating lesions in which neurodegenerative changes have been reported (Kuhlmann et al., 2002), there is also evidence of mild inflammation, such as microglial activation and complement (Barnett and Prineas, 2004) or fibrin (Marik et al., 2007) deposition.

We have used a variant of the experimental autoimmune encephalomyelitis (EAE) model of MS, in which immunization of brown Norway (BN) rats with myelin oligodendrocyte glycoprotein (MOG) results in both general disease signs, such as tail and hindlimb paresis caused by spinal cord lesions, and also the development of optic neuritis in 90% of animals. This is characterized by inflammatory infiltration and demyelination of the optic nerves, accompanied by retinal ganglion cell (RGC) degeneration (Meyer et al., 2001; Hobom et al., 2004; Sättler et al., 2008). Using this model, we aimed to assess the time of onset of neurodegeneration in the retina and determine how retinal neurodegeneration relates to optic nerve histopathology and to inflammatory changes in the retina itself.

Materials and Methods

Rats. Female BN rats (8–10 weeks old; Charles River) were kept under environmentally controlled conditions in the absence of pathogens. All experiments that involved animal use were performed in compliance with the relevant laws and institutional guidelines. These experiments have been approved by the authorities of Saarpfalz-Kreis, Germany.

Received Nov. 14, 2011; revised Feb. 9, 2012; accepted Feb. 24, 2012.

Author contributions: R.F., S.K.W., and R.D. designed research; R.F., S.K.W., D.H., A.S., S.H., and R.D. performed research; F.S. and M.K.S. contributed unpublished reagents/analytic tools; R.F., S.K.W., M.K.S., and R.D. analyzed data; R.F., S.K.W., and R.D. wrote the paper.

This work was supported by the 6th Framework Program of the European Union, NeuroproMiSe Grant LSHM-CT-2005-018637, Gemeinnützige Hertie-Stiftung Grant 1.01.1/09/006, and University of the Saarland Grant HOMFOR 2009. We thank Prof. Hugh Perry for advice regarding cresyl violet staining of retinal whole mounts, Prof. Christine Stadelmann and Prof. Doron Merkler for the kind gift of MOG, and Marika Dienes, Doreen Haar, and Gabriele Kiefer for excellent technical assistance.

*R.F. and S.K.W. contributed equally to this study.

The authors declare no competing financial interests.

Correspondence should be addressed to Dr. Ricarda Diem, Department of Neuro-Oncology, University Clinic Heidelberg, Im Neuenheimer Feld 400, 69120 Heidelberg, Germany. E-mail: ricarda.diem@med.uni-heidelberg.de.

DOI:10.1523/JNEUROSCI.5705-11.2012

 0270-6474/12/325585-13$15.00/0

Induction and evaluation of EAE. Recombinant rat MOG was synthesized as described previously (Weissert et al., 1998). Rats were injected intradermally at the base of the tail with a total volume of 200 μl of emulsion, containing 100 μg of MOG in saline (1:1) with complete Freund's adjuvant (CFA) (Sigma) containing 200 μg of heat-inactivated *Mycobacterium tuberculosis* (strain H 37 RA; Difco Laboratories). Rats were scored daily for clinical signs of EAE as described previously (Meyer et al., 2001). Sham-immunized rats received the same volume of emulsion but without MOG and together with healthy animals served as controls. To control for possible endotoxin contamination of recombinant MOG, samples were analyzed using the Limulus amebocyte lysate assay (Labor L+S), and all were found to contain undetectable levels of endotoxin (<1 IU/ml). In addition, five animals were immunized with recombinant MOG diluted in PBS in the absence of CFA. None of the "MOG-only" control group developed any histopathological abnormalities within the retina or the optic nerves (data not shown).

Retrograde labeling and quantification of RGCs. One week before immunization, RGCs were retrogradely labeled with Fluorogold (Fluorochrome) following a procedure described previously (Hobom et al., 2004). At each time point of 3, 5, 7, and 10 d after immunization and days 1 and 8 of clinical EAE, five rats were perfused with 4% paraformaldehyde (PFA). Retinas were dissected, postfixed in 4% PFA for 20 min, flat-mounted, and examined by fluorescence microscopy (Eclipse E600; Nikon) using a UV filter (365/397 nm) to determine RGC densities (Meyer et al., 2001). Photographs were made with a DXM1200 camera and NIS-Elements software (Nikon).

Cresyl violet staining of retinas. After perfusion of non-Fluorogold-labeled rats, eyes were postfixed in 4% PFA overnight. Retinas were dissected, flat mounted on gelatin-coated slides taking note of orientation, and stained with 0.1% cresyl violet (Perry and Cowey, 1979). The number of cells residing in the ganglion cell layer was then counted. Approximately 50% of the cells in the ganglion cell layer of the rat retina are displaced amacrine cells that do not degenerate after optic nerve transection (Perry, 1981). To estimate the density of the displaced amacrine cells and non-neuronal cells in the ganglion cell layer of the BN rat retina, unilateral optic nerve axotomy was performed to induce RGC death, as described previously (Diem et al., 2001). After 14 d, retinas from axotomized eyes were stained with cresyl violet. Whole-mount sizes were monitored during the staining procedure to avoid artifacts arising from tissue shrinkage.

Optic nerve histopathology. After perfusion of rats with 4% PFA, optic nerves were postfixed in 4% PFA for 24 h and embedded in paraffin. Histological evaluation was performed on 0.5 μm sections stained with Luxol fast blue (LFB) and Bielschowsky's silver impregnation to assess demyelination and axonal pathology, respectively. Demyelinated areas were determined as a percentage of the whole optic nerve cross-section using NIH Image J software. Relative axonal densities were determined in cross-sections of the optic nerves stained by Bielschowsky's silver impregnation by point sampling using a 25-point Olympus eyepiece. Point sampling overcomes the density artifacts that might arise when the optic nerve area is increased as a result of edema (Bitsch et al., 2000). Twenty-five random points were superimposed on the whole of the optic nerve cross-section. The number of points crossing axons was measured as the fraction of the total number of points of the stereological grid. The degree of axon reduction is given as the percentage of axon density compared with the average axon density in healthy optic nerves. IgG deposition was assessed using a biotin-conjugated goat anti-rat IgG antibody (1:200; Jackson ImmunoResearch) and visualization was performed using avidin–biotin detection (ABC Elite kit; Vector Laboratories).

Immunohistochemistry. Immunohistochemistry was performed on optic nerve and retinal sections. After the use of antibodies against CD68 (ED1; 1:500; Serotec), CD3 (1:500; Biozol), and β-amyloid precursor protein (β-APP; 1:1000; Millipore) on paraffin-embedded optic nerve sections, visualization was performed using avidin–biotin detection. Antibodies against CD68 (1:400), aquaporin-4 (AQP-4; 1:800; Millipore), glial fibrillary acidic protein (GFAP) (1:200; Sigma), occludin (1:50; Invitrogen), and albumin (FITC conjugated; 1:20; Abcam; 1:20) were used on frozen retinal sections and paraffin-embedded optic nerves and visualized using Cy3-conjugated secondary antibodies (1:400; Jackson ImmunoResearch). Quantification of CD68- and CD3-positive cells and β-APP-positive axons was achieved using a morphometric grid on a minimum of 10 sections per optic nerve. For terminal dUTP nick end labeling (TUNEL) staining, a modified protocol by Portera-Cailliau et al. (1994) was used. Briefly, frozen retinal sections were treated with proteinase K (20 μg/ml) for 10 min, followed by 3% H_2O_2 for 5 min. Sections were equilibrated in terminal deoxynucleotidyl transferase (TdT) buffer (Roche) before incubated with TdT (Promega) and biotin-16-dUTP (Roche). Positive controls were pretreated with DNase, whereas negative controls lacked biotin-16-dUTP. Sections were visualized using streptavidin–Alexa Fluor 488 (1:750; Invitrogen).

Analysis of spinal cords. Histological evaluation was performed on PFA-fixed, paraffin-embedded spinal cord sections. These were stained with hematoxylin–eosin, LFB, and Bielschowsky's silver impregnation (Storch et al., 1998). Additionally, immunohistochemistry was performed on adjacent serial sections with antibodies against β-APP, CD68, or CD43 (W3/13; 1:1000; Serotec). Visualization was performed using avidin–biotin detection. Quantitative assessment of CD68- or CD43-positive cells, β-APP-positive axons, and semiquantitative analysis of demyelination was determined as described previously (Gadjanski et al., 2009).

Blood–brain barrier integrity. The permeability of the blood–brain barrier (BBB) was determined through Evans blue extravasation. Rats were anesthetized with ketamine and xylazine, and 2% Evans blue in 0.9% NaCl was injected intravenously at a final dosage of 4 ml/kg. Four hours later, rats were perfused with saline to remove intravascular dye. Tissue was then removed for macroscopic analysis using a FZ50 camera (Panasonic) with a DCR-250 macro conversion lens (Raynox).

MOG ELISA. To measure the humoral immune response after MOG immunization, blood was collected and left at 4°C overnight. Serum was isolated by centrifugation for 15 min at 13,000 rpm (4°C, 15,000 × *g*). MOG antibody titers were measured using an ELISA using a 96-well polyvinyl chloride plate coated with the same recombinant MOG used for immunization (0.5 μg/well) by overnight incubation (4°C). After blocking with 5% BSA, the wells were incubated in duplicate with serum probes diluted 1:10,000, 1:100,000, 1:250,000, 1:500,000, and 1:1,000,000 in PBS plus 10% FCS for 2 h at room temperature. After washing with PBS, incubation with HRP-conjugated goat anti-mouse IgG polyclonal antibodies (1:5000; IMGENEX) was performed for 2 h at room temperature. The plate was developed by reaction with 3,3′,5,5′-tetramethylbenzidine (Thermo Fisher Scientific) for 15 min at room temperature and then arrested by addition of 0.1N HCl. The absorbance was read at 450 nm, and, after determination of optimal serum probe dilutions producing a linear response (excluding dilutions that reached saturation or were too low), levels were normalized relative to healthy controls.

Transmission electron microscopy. After perfusion in 1% PFA/2.5% glutaraldehyde in PBS, optic nerves were excised and fixed further in buffered isotonic 2% osmium tetroxide solution for 1 h, followed by dehydration in ethanol and subsequent embedding in epoxy resin. Ultrathin sections (50 nm thick) were cut on an ultramicrotome (UltraCut R; Leica), followed by contrasting with uranyl acetate/lead citrate before analysis on a transmission electron microscope (Tecnai 12 Biotwin; FEI).

Statistics. All data are presented as the mean ± SE. Statistical comparisons were made using Origin 5.0 (OriginLab). For two-group comparisons, the unpaired *t* test was used. A p value of <0.05 was considered statistically significant. All histopathological analyses were performed independently by two investigators in a blinded manner, resulting in no significant differences in counts between investigators. A minimum of five animals were used per time point for each parameter investigated, equating to a minimum of 10 retinas/optic nerves analyzed for each time point.

Results

RGC numbers decrease before onset of clinical EAE

RGC degeneration was assessed by staining the retinas with cresyl violet at various time points after immunization with MOG. On day 1 EAE, the first day when animals had observable symptoms,

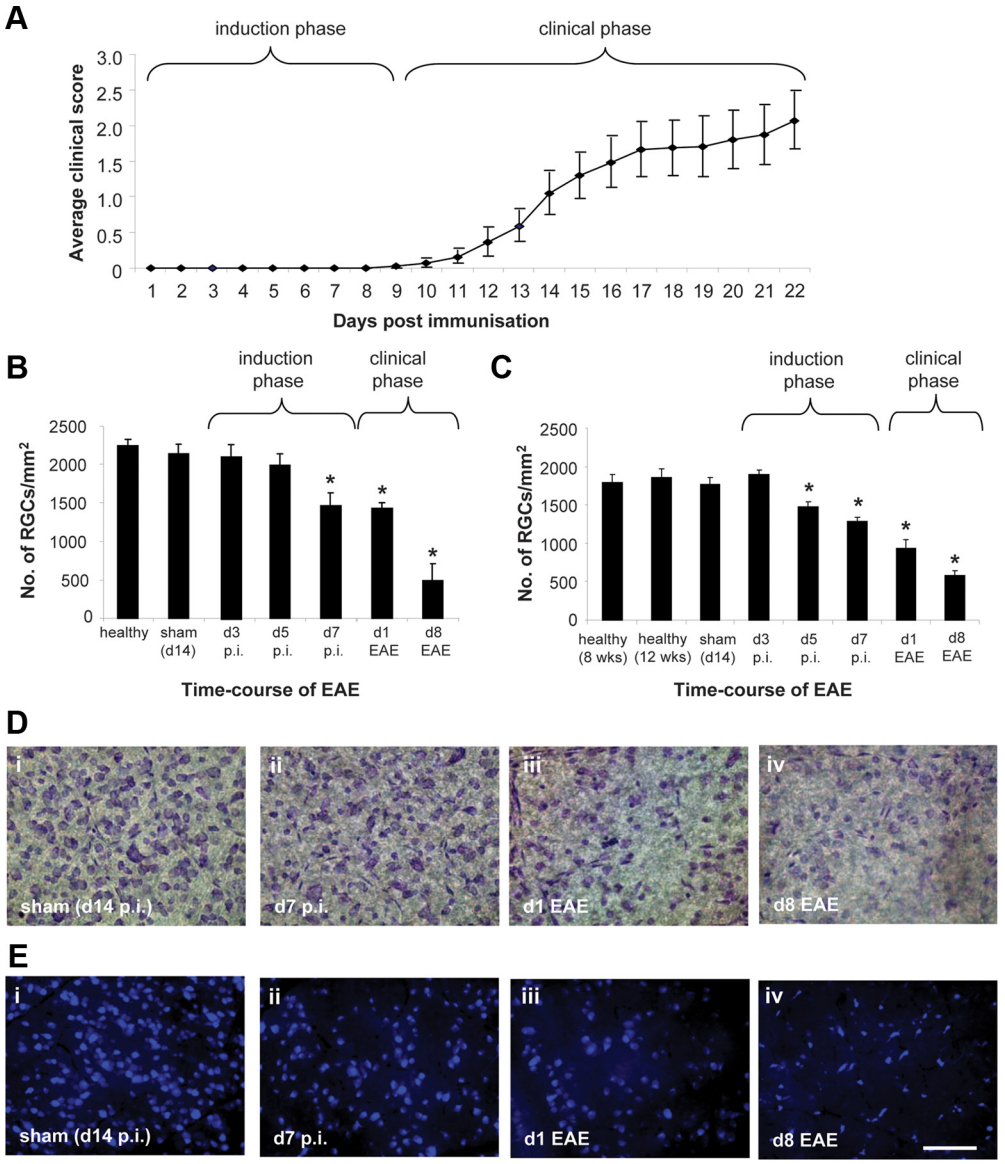

Figure 1. RGC degeneration during EAE. ***A***, Time course of EAE (days after immunization vs clinical EAE score). EAE symptoms were observed at day 10 p.i. at the earliest, although average day of onset was day 14 p.i. ***B***, Numbers of RGCs in cresyl-violet-labeled retinas. Non-RGCs found within the ganglion cell layer, such as displaced amacrine cells, were subtracted from total numbers by subtracting numbers of remaining cells from retinas after optic nerve axotomy was performed. ***C***, Numbers of Fluorogold-labeled RGCs in retinas throughout time course of EAE. ***D***, Example images from cresyl-violet-labeled retinas; sham-immunized (***i***), day 7 p.i. (***ii***), the first day of clinical EAE symptoms (d1 EAE; ***iii***), and 8 d after onset of clinical symptoms (d8 EAE; ***iv***). ***E***, Representative images from Fluorogold-labeled retinas taken from sham-immunized (***i***), day 7 p.i., day 1 EAE (***iii***), and day 8 EAE. *$p < 0.05$, compared with sham. Scale bar, 50 μm.

the average disease score was 0.81 ± 0.12, and, by day 8 EAE, the average disease score was 2.81 ± 0.18 (Fig. 1*A*). To exclude the displaced amacrine cells and small number of non-neuronal cells that reside within the ganglion cell layer, unilateral optic nerve axotomy was performed. Fourteen days after axotomy, almost all RGCs undergo apoptosis (Perry et al., 1984), leaving only the displaced amacrine cells and non-RGCs within the ganglion cell layer. At this time point, the average number of displaced amacrine cells and non-RGCs was counted (2618 ± 114.39 cells/mm^2) and subtracted from cell counts after MOG immunization. A significant decrease in RGC numbers was apparent from day 7 post- immunization (p.i.) (1641 ± 61.4 vs 2046 ± 208.4 cells/mm^2 in healthy animals, $p = 0.009$; Fig. 1*B*). This was several days before onset of clinical EAE, which occurred on average by day 14.27 ± 1.20.

To directly identify the population of RGCs within the retina, Fluorogold was injected into the superior colliculi 1 week before immunization to allow for efficient transport to the cell body. Retinal whole mounts were then prepared throughout the disease course, including control animals taken at a time point before immunization (healthy 8 weeks) and at an age corresponding to MOG-immunized rats running until the end of the experiment (healthy 12 weeks). Using this technique, degeneration of RGCs was observed to be significant as early as day 5 p.i. (1474 ± 66.6 vs 1797 ± 96.6 cells/mm^2 in healthy animals, $p = 0.025$; Fig. 1*C*). It is worth noting that the values obtained by Fluorogold labeling were lower than those from cresyl violet staining. This is presumably attributable to the fact that RGCs terminate not only in the superior colliculi but also the lateral geniculate nuclei (Hofbauer and Dräger, 1985).

In addition, TUNEL staining of the retina was performed (1) to directly assess whether RGCs underwent apoptosis, confirming that cells within the ganglion cell layer started to degenerate as early as day 5 p.i. (see Fig. 9*J*) and (2) to address whether degen-

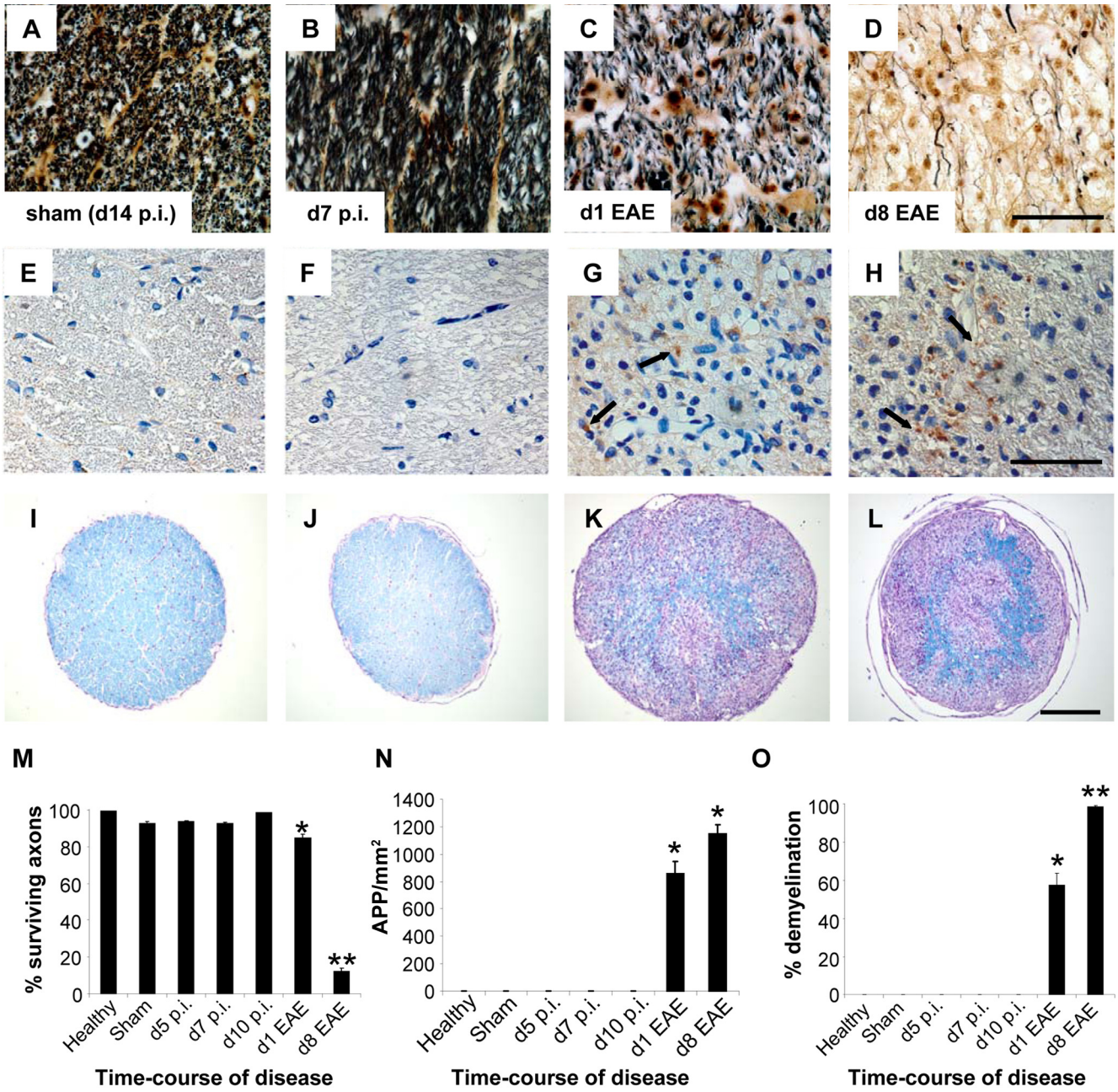

Figure 2. Axonal pathology. ***A–D***, Axonal density was examined in optic nerve cross-sections using Bielschowsky's silver stain. Representative images were taken from a sham-immunized rat 14 d after immunization (sham) (***A***), day 7 p.i. (***B***), day 1 EAE (***C***), and day 8 EAE (***D***). ***E–H***, Representative images of β-APP accumulation in optic nerves from sham-immunized (***E***), day 7 p.i. (***F***), day 1 EAE (***G***), and day 8 EAE (***H***). ***I–L***, Demyelination was assessed by LFB to label myelin. Representative images were taken from sham-immunized (***I***), day 7 p.i. (***J***), day 1 EAE (***K***), and day 8 EAE (***L***). Quantification was performed for axonal density (***M***), β-APP accumulation (***N***), and demyelination (***O***). $^*p < 0.05$; $^{**}p < 0.01$, compared with sham. Scale bars: ***D***, ***H***, 50 μm; ***L***, 200 μm.

eration was restricted to this layer. At day 5 p.i., TUNEL-positive cells were seen mainly in the ganglion cell layer, but some labeling was also apparent within the inner and outer nuclear layers, becoming more frequent by day 10 p.i.. This observation is in agreement with findings reported in retinas from MS patients in which retinal degeneration was also reported in the ganglion and inner nuclear layers (Green et al., 2010).

Thus, through use of various methods to assess RGC degeneration, loss of RGC bodies was seen to be an early event, preceding by several days the onset of clinical EAE. Sham-immunized controls were taken on day 14 p.i. and did not have reduced numbers of RGCs.

RGC axon density decreases with onset of EAE

To assess axonal integrity, optic nerves were taken at various time points and cross-sectioned (Fig. 2). The density of axons within the optic nerves, demonstrated by Bielschowsky's silver staining, correlated strongly with the degree of demyelination, shown by LFB (Fig. 2*M*,*O*). Note the increase in optic nerve cross-section sizes at clinical time points, presumably as a result of edema (also see Fig. 8*I*,*J*). To assess acute axonal injury, accumulation of β-APP was measured. However, axonal loss, demyelination, and β-APP accumulation were not observed until day 1 of clinical EAE (Fig. 2*N*), occurring as much as 1 week after the onset of RGC loss. This correlated with observations from assessment of

Table 1. Summary of histopathological analyses of the spinal cord (mean ± SEM)

	DM score	ED1/mm^2	W3/13/mm^2	β-APP/mm^2
Healthy	0.00 ± 0.00	0.00 ± 0.00	0.00 ± 0.00	0.00 ± 0.00
Sham	0.00 ± 0.00	0.60 ± 0.38	0.00 ± 0.00	0.00 ± 0.00
Day 3 p.i.	0.00 ± 0.00	0.10 ± 0.10	0.00 ± 0.00	0.00 ± 0.00
Day 5 p.i.	0.00 ± 0.00	0.00 ± 0.00	0.00 ± 0.00	0.00 ± 0.00
Day 7 p.i.	0.00 ± 0.00	0.20 ± 0.20	0.00 ± 0.00	0.00 ± 0.00
Day 10 p.i.	0.00 ± 0.00	0.18 ± 0.18	0.17 ± 0.17	0.00 ± 0.00
Day 1 EAE	1.00 ± 1.00	32.47 ± 5.82	18.51 ± 17.39	5.07 ± 3.24
Day 8 EAE	1.08 ± 0.46	80.58 ± 44.76	11.96 ± 9.58	3.90 ± 2.29

Summary of demyelination, inflammation, and acute axonal injury in the spinal cord throughout the preclinical phase and after the onset of EAE. Demyelination was evaluated semiquantitatively as described (Gadjanski et al., 2009) (DM score). Quantitative analyses of the number of ED1-positive cells (activated microglia/macrophages), W3/13-positive cells (T-cells), and acutely damaged β-APP axons were calculated per square millimeter of the total cross-section of the spinal cord.

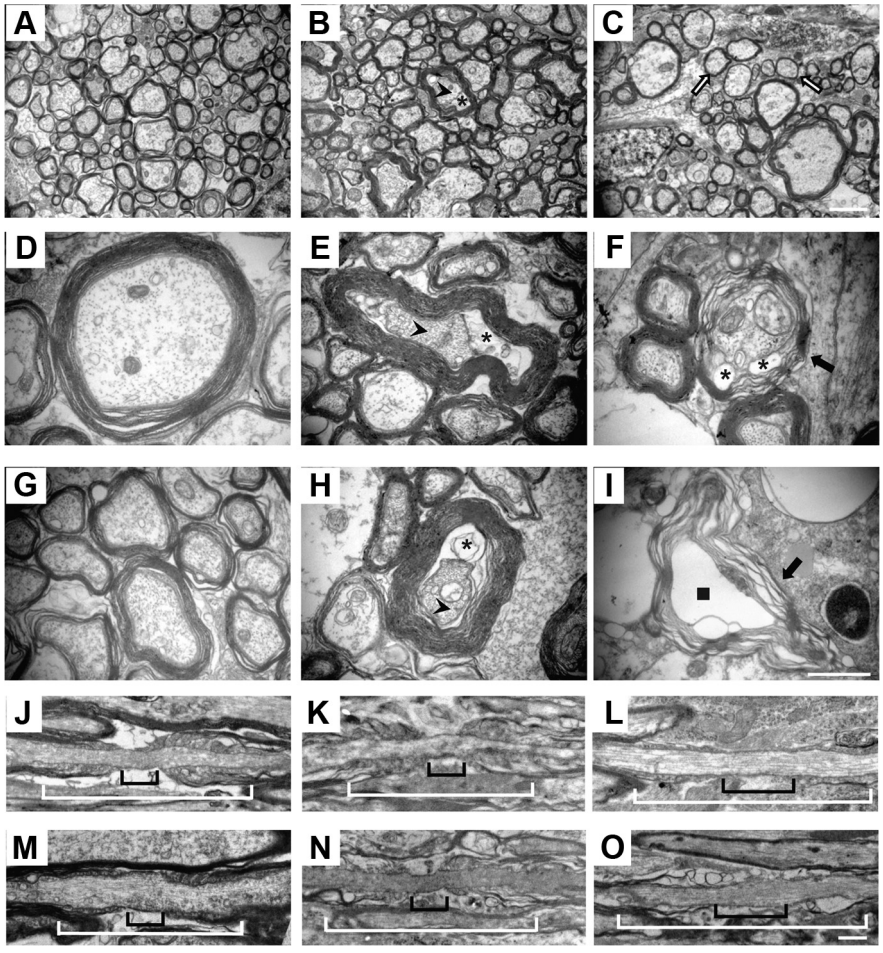

Figure 3. Ultrastructure of optic nerves. Electron microscopy was performed on ultrathin cross-sections of the optic nerve. Representative images are shown from healthy (***A***), day 7 p.i. (***B***), and day 1 EAE (***C***). Higher-magnification images of representative axons are also shown from healthy (***D***, ***G***), day 7 p.i. (***E***, ***H***), and day 1 EAE (***F***, ***I***) animals. Longitudinal images of nodes of Ranvier are shown from healthy (***J***, ***M***), day 7 p.i. (***K***, ***N***), and day 1 EAE (***L***, ***O***) animals. Asterisks denote vacuoles between the axolema and myelin sheath, arrowheads denote condensed axons, white arrows denote axons with thin myelin, black arrows denote axons with uncompacted myelin, and black square denotes myelin ring lacking a central axon. Black bar marks the intra-nodal region, whereas the white bar marks the whole node (intranodal and paranodal regions). Scale bars: ***C***, 2 μm; ***I***, ***O***, 1 μm.

the spinal cord (Table 1) in which each of these parameters were unchanged compared with healthy and sham controls until day 1 EAE.

Because there was no evidence of axon degeneration or demyelination during the preclinical phase, electron microscopy was performed on optic nerve sections taken during disease onset to assess any ultrastructural alterations. In agreement with the histopathological results, axons remained fully myelinated during the preclinical phase (Fig. 3*B*). In addition, the length of nodes of Ranvier appeared to be unchanged at day 7 p.i. (Fig. 3*K*,*N*). However, despite the presence of intact myelin, there were signs of axonal degeneration (Fig. 3*E*,*H*). Many axons appeared shrunken, and vacuoles could be seen between the axolema and myelin sheath. By the day of disease onset, after assessing the axonal ultrastructure within still myelinated regions, many axons had thin or uncompacted myelin (Fig. 3*C*,*F*), with some myelin bundles lacking the presence of axons altogether (Fig. 3*I*). In addition, both intranodal and paranodal distances were seen to be enlarged (Fig. 3*L*,*O*). Thus, although inflammatory infiltration and myelin pathology during the preclinical phase of optic neuritis was not observed, axonal degeneration can be seen to have already begun correlating with degeneration of RGC bodies within the retina.

RGC death precedes immune responses

The timing of the cellular immune response after MOG immunization was determined by identifying when CD3-positive T-cells infiltrated the optic nerve parenchyma (Fig. 4*E*). No significant levels of CD-3-positive cells were observed until day 1 EAE, when infiltrating T-cells were detected (170.13 ± 66.45 cells/mm^2). However, in samples taken between days 5 and 10 p.i., small numbers of CD3-positive T-cells could be identified in the optic nerve meninges (Fig. 4*G*) and in the outer layers of the retina, in particular the choroid. This was seen in sections from all time points analyzed (Fig. 4*J*,*K*).

The timing of the humoral immune response was assessed by measurement of anti-MOG antibodies in the blood. An ELISA against MOG demonstrated significantly elevated levels of anti-MOG antibodies by day 10 p.i. (3.89 ± 1.03 times higher than healthy, $p = 0.038$; Fig. 4*F*), which continued to rise as the clinical phase of the disease progressed. This rise, however, was not observed until after the onset of RGC degeneration. Similarly, visualization of deposited IgG (presumably anti-MOG) was detectable in the optic nerve head (ON-H) only from day 10 p.i., in agreement with the ELISA results, becoming much more widespread at day 1 EAE (Fig. 4*L*–*O*). The ON-H was assessed because of its open BBB (see Fig. 6*A*), allowing any circulating antibodies to be deposited and visualized.

Breakdown of the blood–retinal barrier coincides with the onset of RGC degeneration

To determine the timing of alterations in BBB permeability, Evans blue extravasation was performed throughout the induction and clinical phases of EAE. Macroscopic analysis of CNS tissue showed Evans blue extravasation in all compartments investi-

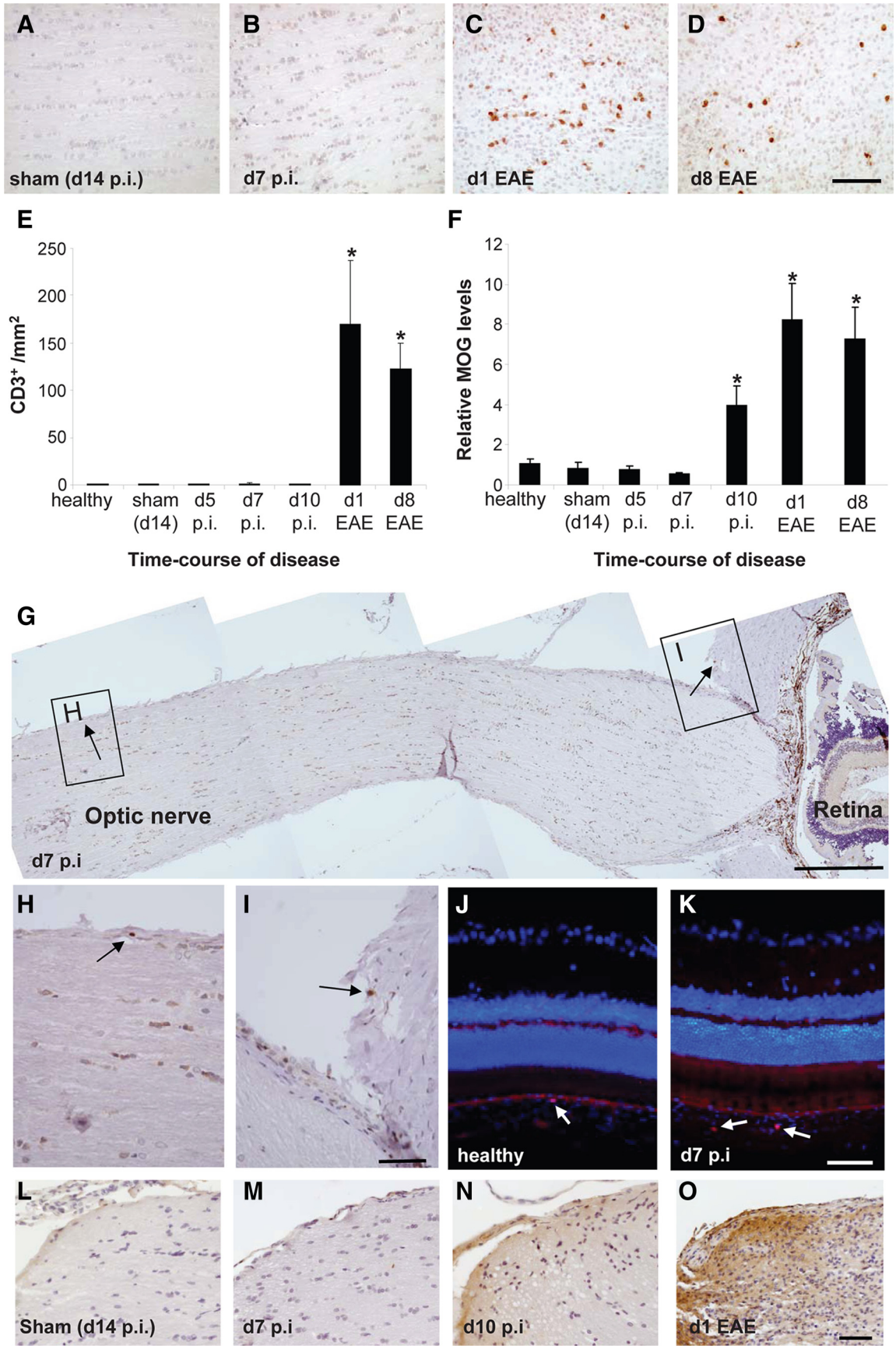

Figure 4. T-cell/B-cell response. Immunohistochemistry against CD3 to label T-cells was performed in optic nerve sections. Representative images were taken from a sham-immunized rat (***A***), day 7 p.i. (***B***), day 1 EAE (***C***), and day 8 EAE (***D***). ***E***, Numbers of infiltrating CD3-positive T-cells were quantified at the different time points after immunization. ***F***, An (*Figure legend continues.*)

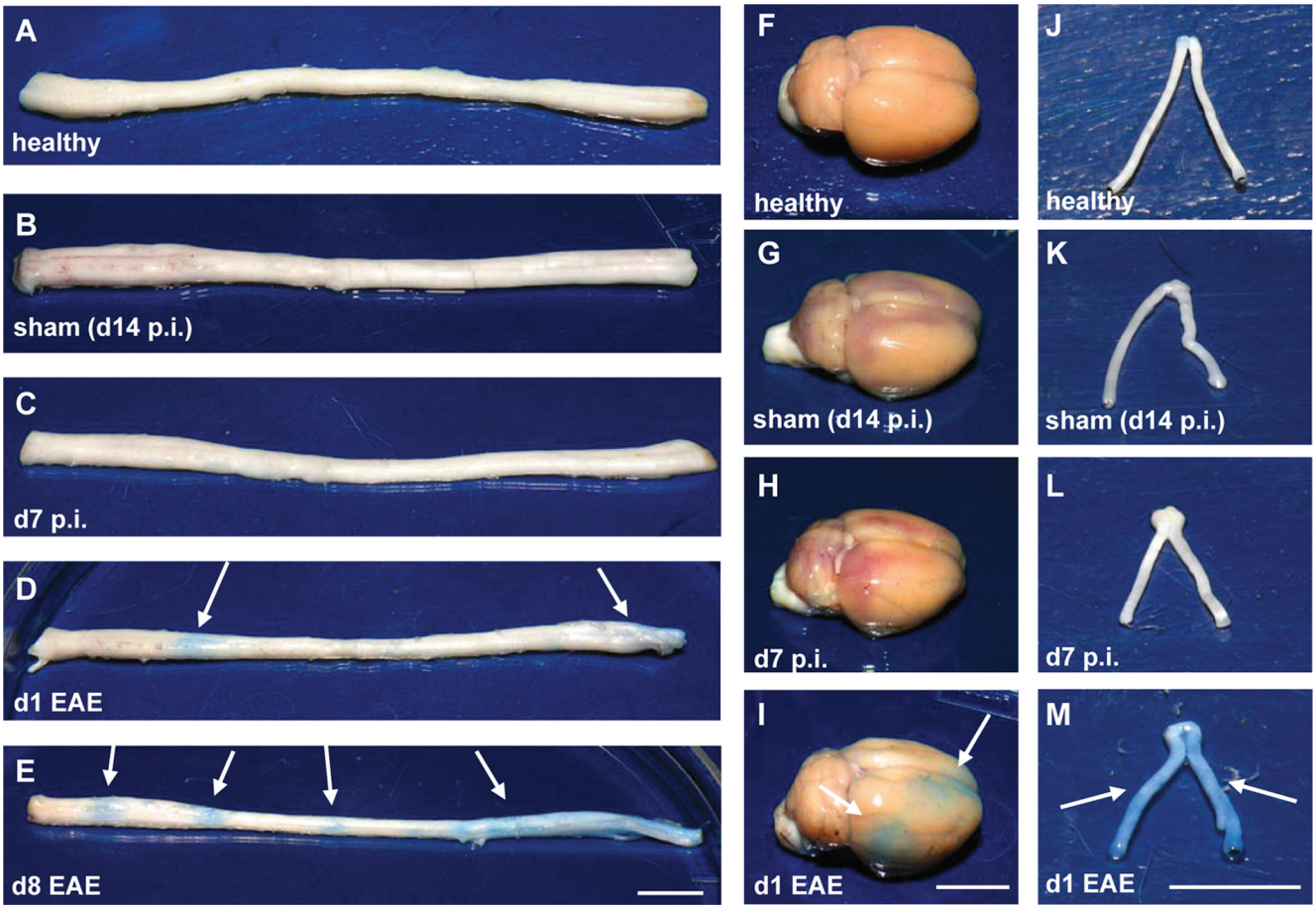

Figure 5. Macroscopic analysis of Evans blue extravasation. To determine when and where the BBB is broken down, Evans blue dye was injected intravenously into the lateral tail vein. After 4 h, rats were perfused with saline, and spinal cord, brain, and optic nerves were dissected and visualized. Blue areas of Evans blue extravasation, showing where Evans blue leaked through the BBB into surrounding tissue, were only observable from day 1 EAE onward. Spinal cord (***A–E***), brain (***F–I***), and optic nerves (***J–M***) were taken from animals that were healthy (***A***, ***F***, ***J***), sham-immunized (***B***, ***G***, ***K***), day 7 p.i. (***C***, ***H***, ***L***), or day 1 (***D***, ***I***, ***M***) or 8 (***E***) after clinical symptoms develop. Arrows indicate areas of blue dye accumulation in the tissue. Scale bar, 10 mm.

gated at day 1 EAE but not during the earlier induction phase (Fig. 5). Leakage was particularly strong in both spinal cord and optic nerves (Fig. 5*D*,*M*), although some areas of Evans blue extravasation were also apparent in the brain (Fig. 5*I*).

To investigate BBB permeability in more detail, immunohistochemistry was performed on frozen optic nerve sections with a FITC-conjugated antibody against albumin. After assessing the whole length of healthy optic nerves, albumin leakage could be seen at the ON-H (Fig. 6*A*), in agreement with previous reports that the BBB is incomplete here (Tso et al., 1975; Hu et al., 1998). However, along the rest of the optic nerve, albumin was only detected within blood vessels. Counterstaining against AQP-4 to label astrocytic end feet aided assessment of the fine structure of the BBB. No albumin extravasation was seen in optic nerves during the induction phase of EAE, but at day 10 p.i., AQP-4 staining was irregular (Fig. 6*H*), becoming more diffuse during the clinical phase of EAE (Fig. 6*K*). It is possible that the irregular pattern of AQP-4 could represent the earliest dysregulation of the BBB, which subsequently becomes permeable by day 1 EAE. This is supported by the observation of a dysregulated distribution of the tight junction protein, occludin, from day 10 p.i onward (Fig. 6*N*,*Q*).

In the healthy retina, sealed blood vessels were apparent (Fig. 7*A*,*P*,*Q*) by anti-albumin staining. AQP-4 was again used as a counterstain. However, leakage of the blood–retina barrier (BRB) was observable during the induction phase with small amounts of albumin extravasation visible from day 5 p.i. (Fig. 7*D*) and large amounts by day 7 p.i. (Fig. 7*G*). By day 1 EAE, albumin staining of vessels was much weaker and albumin extravasation could be seen across large sections of the retina (Fig. 7*M*), suggesting a fully permeable BRB at this stage. This correlated with a distinct disruption of AQP-4 labeling by day 1 EAE, again demonstrating the disturbance in BRB integrity. The timing of opening of the BRB correlates closely with the onset of RGC degeneration (Fig. 1*C*).

Astrocytic reactivity was also assessed in retinas through the disease course. GFAP reactivity was seen in the nerve fiber layer of healthy and sham-immunized retinas, and reactive astrocytic labeling could be seen from day 5 p.i. onward (see Fig. 9*G*), increasing through to the onset of EAE (see Fig. 9*H*). In conclusion, GFAP upregulation correlated with both the timing of AQP-4 disruption and albumin extravasation.

←

(*Figure legend continued.*) ELISA to detect MOG antibodies was performed on serum collected from rats at different time points after immunization and from healthy and sham-immunized rats. ***G***, A representative section through the ON-H and retina (day 7 p.i.) showing two CD3-positive T-cells within the meninges. ***H***, ***I***, Magnified images of boxed areas in ***G***. ***J***, ***K***, Retinal sections from healthy (***J***) and day 7 p.i. (***K***) retinas showing presence of CD3-positive T-cells within the choroid of the retina. Ganglion cell layer is uppermost layer (DAPI, blue; CD3, red). ***L–O***, Representative images of IgG deposition in the ON-H of sham-immunized (***L***), day 7 p.i. (***M***), day 10 p.i. (***N***), and day 1 EAE (***O***) optic nerves. $^*p < 0.05$, compared with sham. Scale bars: ***D***, ***K***, ***O***, 50 μm; ***G***, 500 μm; ***I***, 100 μm.

Early microglial activation in autoimmune optic neuritis

Optic nerve and retinal sections were stained with an antibody against CD68 to detect activated microglia and macrophages. In the optic nerve, large numbers of CD68-positive cells were apparent in sections taken from animals with clinical symptoms (Fig. 8*C*,*G*). These cells were morphologically reminiscent of macrophages because of their large and foamy appearance. However, after examination of the induction period of the disease, small but significantly elevated numbers of CD68-positive cells were observed as early as day 5 p.i. (12.44 ± 1.66 vs 6.00 ± 1.35 cells/mm^2 in healthy optic nerves, $p = 0.041$; Fig. 8*H*) but were not elevated in sham-immunized animals. Because of morphological criteria, such as retracted processes and smaller size, these are likely to be reactive microglia (Fig. 8*E*). Again, this is a close correlate of RGC degeneration. After analyzing the distribution of these CD68-positive cells in both the induction and clinical phases, it could be seen that larger numbers were present in the vicinity of the ON-H, which decreased proportionally with increased distance along the optic nerve (Fig. 8*I–K*).

A similar increase in CD68-positive cells was also seen in the retina, in which by day 5 p.i. significantly elevated numbers were observed (4.60 ± 0.23 vs 3.26 ± 0.42 cells/mm length in sham-immunized retinas, $p = 0.039$; Fig. 9*E*). No significantly elevated numbers of CD68-positive cells were seen at any of the sham-immunized time points (Fig. 9*A*,*E*). This elevation closely correlated with the timing of BRB breakdown (Fig. 7). Spinal cords were also investigated, but although CD68-positive cells were elevated from day 1 EAE, no significant increases were seen during the induction phase (Table 1).

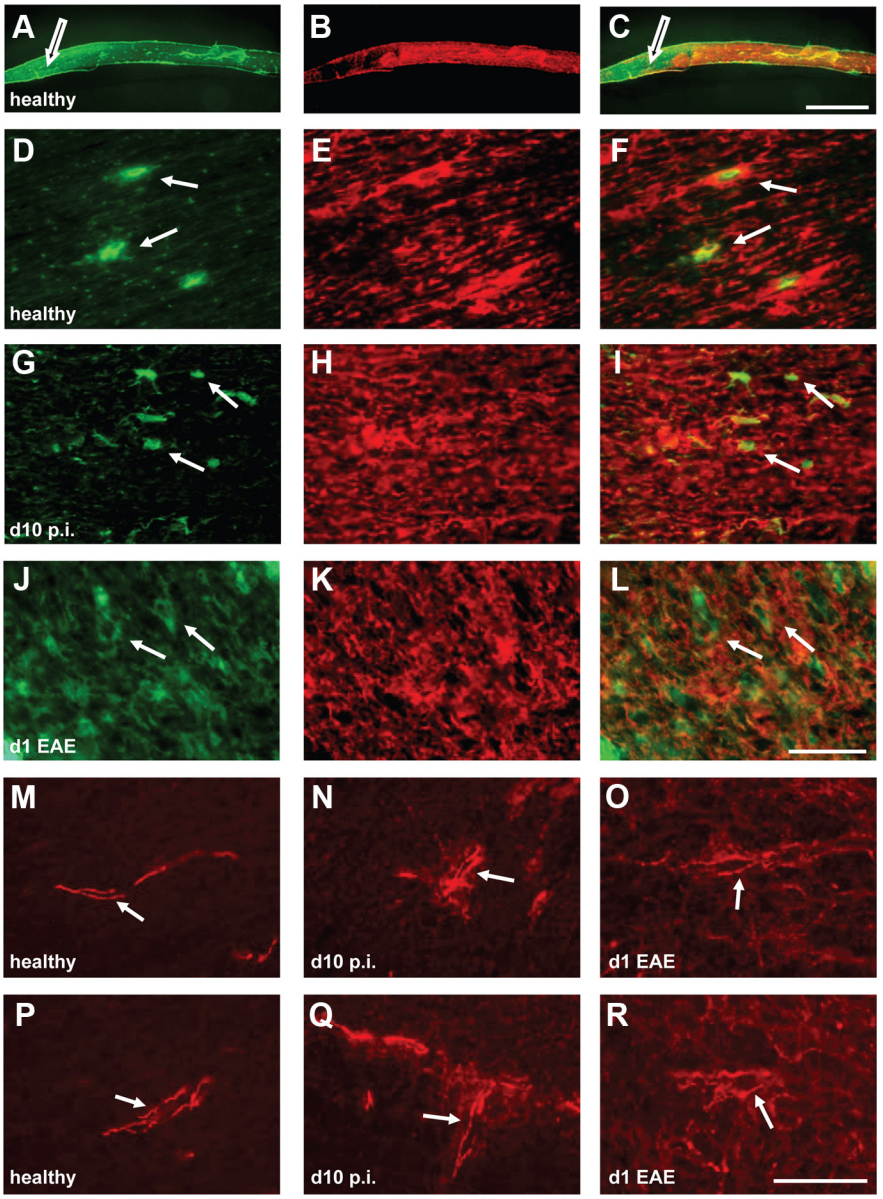

Figure 6. BBB integrity in optic nerves. Optic nerve sections were colabeled with an antibody against albumin (green) to label areas of blood leakage (***A***, ***D***, ***G***, ***J***) and AQP-4 to label astrocytic end feet surrounding blood vessels (***B***, ***E***, ***H***, ***K***). Merged images are given in ***C***, ***F***, ***I***, and ***L***. ***A–C***, Healthy nerve at low magnification shows BBB permeability toward the ON-H (open arrows). Healthy (***D–F***), day 10 p.i. (***G–I***), and day 1 of EAE (***J–L***), demonstrating more disrupted AQP-4-labeled structures from day 10 p.i., whereas blood vessel permeability is observed from day 1 EAE. White arrows indicate areas of accumulated albumin. ***M–R***, Immunofluorescent labeling against the tight junction protein occludin on healthy (***M***, ***P***), day 10 p.i. (***N***, ***Q***), and day 1 EAE (***O***, ***R***) optic nerves. White arrows indicate blood vessels. Scale bars: ***C***, 200 μm; ***L***, ***R***, 50 μm. High-magnification images were taken at a distance of 500 μm from the lamina scleralis of the ON-H.

Discussion

We show that RGC degeneration is an early event after immunization with MOG, preceding the onset of clinical EAE. In addition, we show that RGC bodies are lost before their axons, which, at the time of significant RGC loss, still appear in full numbers but with signs of degeneration detectable at the ultrastructural level. These findings might indicate that the cause/trigger appears to develop within the retina and is not secondary to optic nerve injury, as is believed to occur during the clinical phase of the disease (Trapp et al., 1998; Meyer et al., 2001; Dutta and Trapp, 2007). Additionally, we observe no demyelination or infiltration of immune cells into the optic nerve parenchyma during the induction phase of optic neuritis, although small numbers of T-cells could be observed in the optic nerve meninges and choroid of the retina. It must be noted, however, that subclinical changes found to be present in the optic nerve may still be responsible for onset of degeneration, as has been suggested in other retinal disorders, such as glaucoma in which mounting evidence suggests that changes in the proximal optic nerve may instigate additional degeneration of the retina (Grieshaber and Flammer, 2007; Soto et al., 2011). Thus, it remains an open question whether retinal or optic nerve pathology is the predominant cause, thus defining whether primary or secondary degeneration is actually taking place. This is particularly intriguing with respect to the lack of MOG in the retina. In accordance with this, evidence of BRB breakdown and activation of resident microglia in both the retina and optic nerve was seen during this early disease stage, in parallel with RGC degeneration.

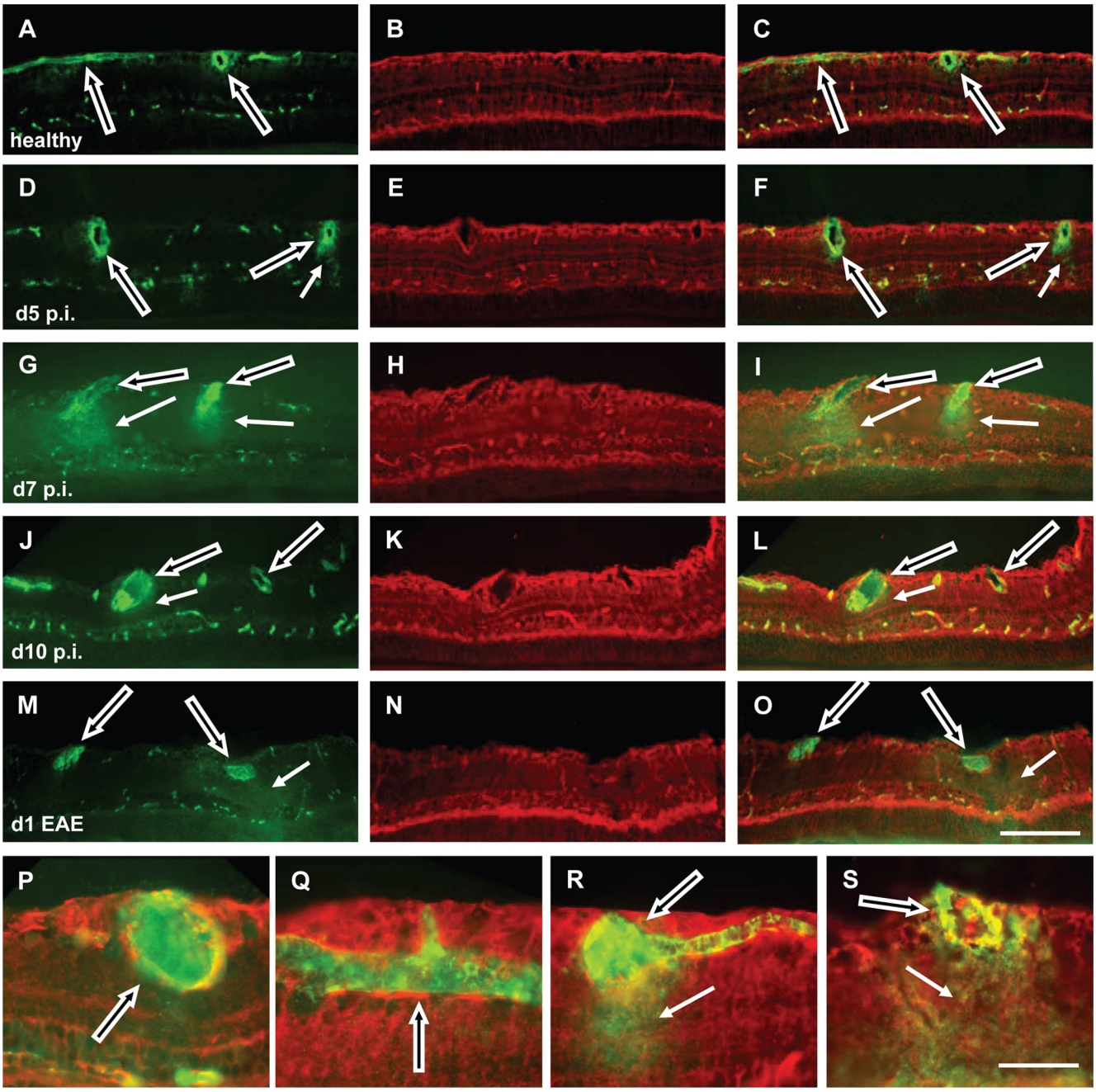

Figure 7. BRB integrity. Retinal sections were colabeled with an antibody against albumin (green) to label areas of blood leakage (***A***, ***D***, ***G***, ***J***, ***M***) and AQP-4 to label astrocytic end feet surrounding blood vessels (***B***, ***E***, ***H***, ***K***, ***N***). Merged images are given in ***C***, ***F***, ***I***, ***L***, ***O***, ***P–S***). Healthy (***A–C***), day 5 p.i. (***D–F***), day 7 p.i. (***G–I***), day 10 p.i. (***J–L***), and day 1 EAE (***M–O***). Open arrows indicate blood vessels, and filled arrows indicate areas of accumulated albumin. High-magnification representative images are given of closed blood vessels (***P***, ***Q***, healthy retinas) and leaky blood vessels (***R***, day 7 p.i.; ***S***, day 1 EAE) from within the ganglion cell layer. Scale bars: ***O***, 100 μm; ***S***, 50 μm.

The mechanism by which neurodegeneration is induced is likely to be a result of one or more of the following: activation of the innate immune response or activation of either the humoral or cellular arms of the adaptive immune response. A close correlation in both the activation of microglia/macrophages and breakdown of the BRB was observed with the onset of neurodegeneration, suggesting a relationship between these events. However, RGC degeneration in our model seems to be a MOG-dependent event because it did not occur in sham-immunized animals. In this context, it could be hypothesized that MOG-specific antibodies are involved both in induction of neurodegeneration and activation of resident microglia within the optic nerves and retina. However, our data demonstrated that significantly elevated levels of systemic anti-MOG antibody were not detected in the serum until day 10 p.i., several days after the onset of both neurodegeneration and microglia activation. Thus, it appears unlikely that MOG-specific antibodies would fulfill this role, although it remains a possibility that the sensitivity of the ELISA was insufficient to detect low antibody levels. An additional possible mechanism explaining the MOG specificity of neurodegeneration relates to the role of T-cells. T-cells were observed, although only in low numbers, in both the meninges of the optic nerves and choroid of the retina during the preclinical phase. However, it remains to be explained how MOG-specific

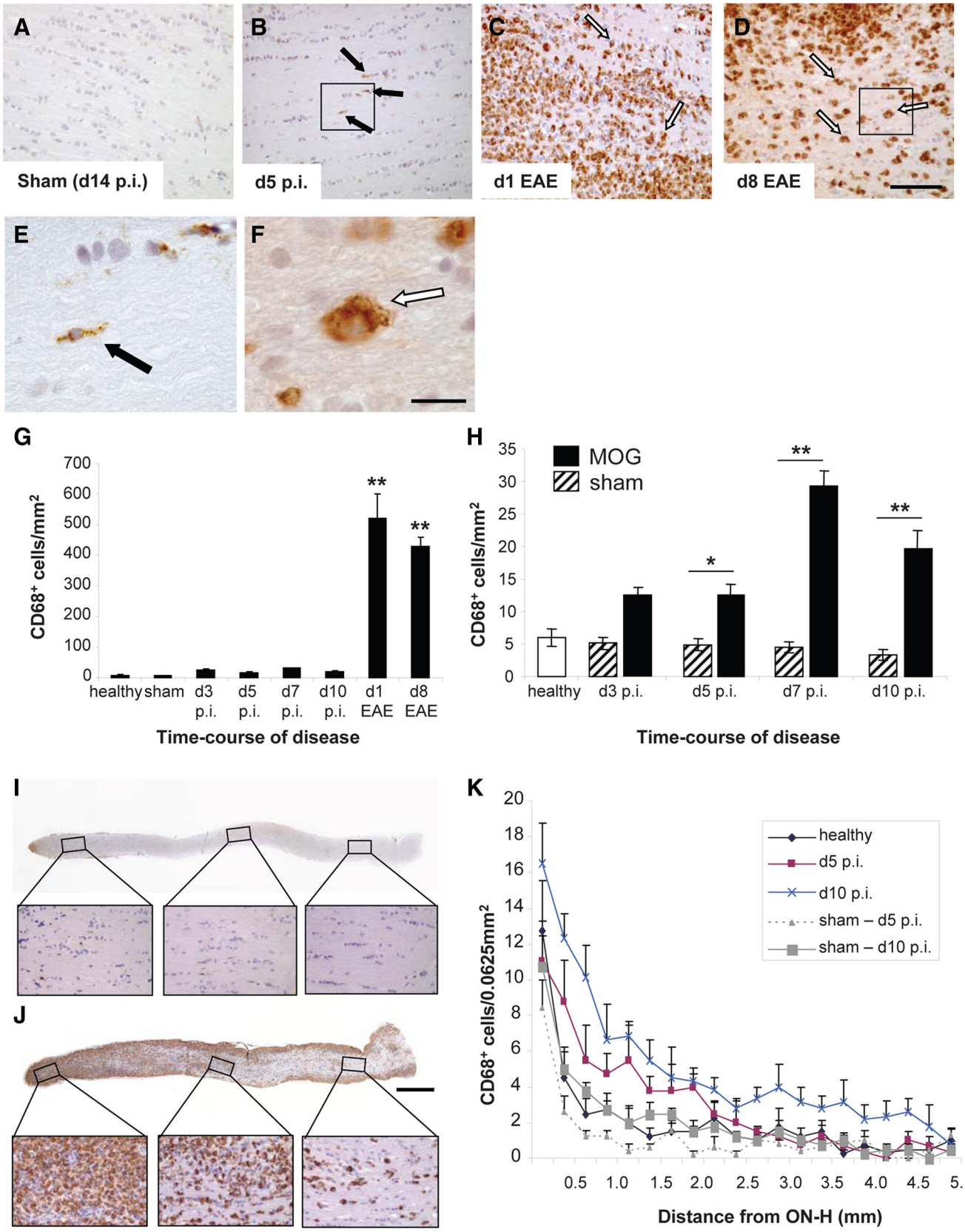

Figure 8. Activated microglia and macrophages in optic nerves. ***A–D***, Optic nerve sections were stained with an antibody against CD68 to label microglia and macrophages. Representative sections are shown from sham-immunized (***A***), day 5 p.i. (***B***), day 1 EAE (***C***), and day 8 EAE (***D***). ***E***, ***F***, Magnified examples of microglia-like (black arrows) and macrophage-like (white arrows) morphology of CD68-positive cells taken from boxed areas in ***B*** and ***D***, respectively. ***G***, Quantification of CD68-positive cells per square millimeter throughout EAE time course. ***H***, Quantification of CD68-positive cells during induction phase of disease. Low-magnification images of longitudinal optic nerve sections from day 5 p.i. (***I***) and day 1 EAE (***J***), showing distribution of CD68-positive cells. Boxed areas show magnified views of areas indicated. ***K***, Quantification of CD68-positive cell distribution along length of optic nerves. *$p < 0.01$, **$p < 0.001$, compared with respective sham values. Scale bars: ***D***, 50 μm; ***F***, 10 μm; ***J***, 200 μm.

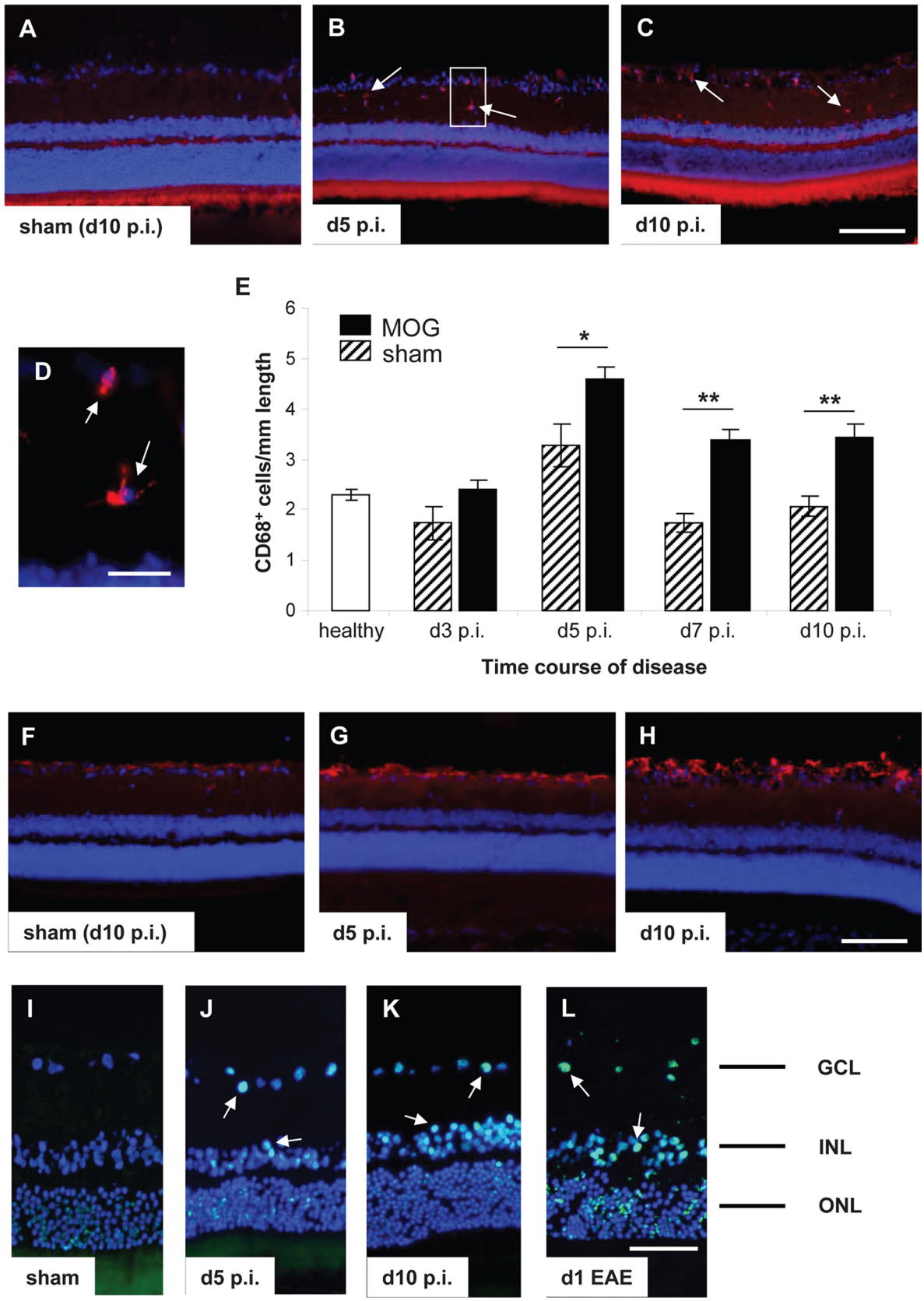

Figure 9. Activated microglia and macrophages in retina. ***A–D***, Retinal sections were stained with an antibody against CD68. Representative images are shown from sham-immunized (***A***), day 5 p.i. (***B***), and day 10 p.i (***C***), with labeled CD68-positive cells indicated with arrows. ***D*** is an enlarged view of the boxed area in ***B***. Tissue was counterstained with DAPI (blue) to aid identification of retinal layers (ganglion cell layer is uppermost DAPI monolayer); anti-CD68-labeling is in red. ***E***, Quantification of CD68-positive cells per millimeter length throughout induction phase of disease. ***F–H***, Immunohistochemistry for GFAP from sham-immunized (***F***), day 5 p.i. (***G***), and day 10 p.i. (***H***). $*p < 0.05$, $**p < 0.01$, compared with respective sham values. ***I–L***, TUNEL-labeled retinas (green) with DAPI counterstain (blue) from sham-immunized (***I***), day 5 p.i. (***J***), day 10 p.i. (***K***), and day 1 EAE (***L***) animals. Arrows indicate apoptotic nuclei. Scale bars: ***C***, ***H***, 100 μm; ***D***, 20 μm; ***K***, 50 μm. GCL, Ganglion cell layer; INL, inner nuclear layer; ONL, out nuclear layer.

T-cells could mediate neurodegeneration in the MOG-deficient retina. One possibility might be MOG-associated epitope spreading because, in a mouse model of EAE, MOG-reactive T-cells have been found to recognize neuronal proteins, such as neurofilament-M (Krishnamoorthy et al., 2009). In addition, another study has reported a dual response of MOG-reactive T-cells against two target auto-antigens in different tissues (Stefferl et al., 2000). This would be an important confounder of this model, raising the possibility that MOG-activated T-cells may find potential neuronal targets even in MOG-deficient areas.

Additional insights into the interconnection between immune activation and RGC degeneration may also be obtained by comparison with findings in the retinal disease models of glaucoma or uveitis. In both cases, macrophage recruitment into the retina and BRB disturbances occur (Bhattacherjee et al., 1983; McMenamin and Crewe, 1995; Golubnitschaja et al., 2002; Grieshaber and Flammer, 2007), accompanied by degeneration of RGCs (Quigley, 1999; El-Remessy et al., 2008). In addition, glaucoma-linked activation of the complement cascade has also been shown to induce both synaptic loss and apoptosis (Stevens et al., 2007; Jha et al., 2011).

Activation of retinal microglia has been described as a common early event in many retinal conditions (Langmann, 2007), in which resident microglia may be uniquely sensitive to changes in their microenvironment (Schuetz and Thanos, 2004). Whether activated microglia are necessary to induce damage to blood vessel integrity, or alternatively, soluble factors such as cytokines or antibodies are able to penetrate from damaged blood vessels to stimulate microglial activation is at present unclear, although the correlation between density and distribution of activated optic nerve microglia with the permeable ON-H suggest that diffusion of such factors into the optic nerve might be required. However, because of the timing of both events with the onset of RGC degeneration, it is a distinct possibility that they are both involved with induction of RGC apoptosis.

Although we report retinal pathology in an animal model of MS, we believe they are highly relevant to the human condition. A growing number of studies published within the past few years have highlighted retinal affection in MS through analysis of retinal nerve fiber layer (RNFL) and macular thinning by optical coherence tomography (Fisher et al., 2006; Gordon-Lipkin et al., 2007; Pulicken et al., 2007; Saidha et al., 2011) and retinal atrophy in autopsy material (Green et al., 2010). Significantly, the RNFL has also been shown to be thinner in eyes of MS patients who have not been clinically affected by optic neuritis (Fisher et al., 2006; Henderson et al., 2008), leading to the suggestion that RFNL thinning may represent neurodegeneration on a more global level because it has been shown to correlate with brain atrophy (Frohman et al., 2006; Gordon-Lipkin et al., 2007). Additionally, it has been proposed that neuronal pathology might develop in the retina independent of optic nerve changes (Saidha et al., 2011). Using animal models to complement observations of retinal pathology in human MS patients is significant because it enables the investigation of underlying disease mechanisms on a histological level and during acute or even pre-acute disease stages.

Additional indications of neurodegeneration in the absence of inflammatory demyelination in MS come from the observation of axonal damage in NAWM (Bitsch et al., 2000; Kornek et al., 2000). During the development of NAWM lesions, clusters of activated microglia have been observed in the absence of demyelination, and it has been speculated that these represent an early event in the formation of a lesion (De Groot et al., 2001; Peterson et al., 2001; van der Valk and Amor, 2009). This has been confirmed in other studies in which, after characterizing lesions according to time since disease onset, an initial stage involving microglia activation was seen before T-cell infiltration and demyelination (Gay et al., 1997; Barnett and Prineas, 2004).

However, before the infiltration of T-cells into the CNS parenchyma, the presence of meningeal T-cell infiltrates has been observed and shown to be another early event in the development of EAE lesions (Traugott et al., 1978; Tsuchida et al., 1994). Similar mechanisms appear to be supported by the observation of inflammatory infiltrates in the perivascular space of NAWM of patients with type III demyelinating lesions (Marik et al., 2007). The authors suggest that these perivascular T-cells, which correlate with the numbers of activated microglia, may mediate BBB disturbances facilitating the activation of microglia, possibly by influx of fibrin or proinflammatory cytokines. This may also explain why we saw more activated microglia in the vicinity of the permeable ON-H, because the entry of cytokines and other diffusable factors from the vasculature may be occurring more readily in this region. Although we did not observe any T-cells within the perivasculature of the optic nerve or retina in our study, as a result of the low numbers involved, we cannot rule it out. Thus, meningeal, and potentially perivascular, T-cells may provide a mechanism for the activation of resident microglia in our model before the onset of clinical EAE symptoms.

In conclusion, there has been much discussion as to whether MS should be reinterpreted as a neurodegenerative disease rather than primarily as a demyelinating disease (Trapp and Nave, 2008). Evidence includes the fact that, in the myelin-deficient retina, neurodegeneration has been reported to be more widespread than observations of focal inflammation (Green et al., 2010). Although these neurodegenerative events are not occurring in the absence of inflammation, as evidenced by a recent report showing the close correlation between inflammation and neurodegeneration in MS lesions of all stages (Frischer et al., 2009), lymphocytic myelin attack is not the only causative event. In this context, our data support a growing viewpoint that, before lymphocytic invasion of CNS tissue, the innate immune system may play a critical role in mediating early neurodegeneration.

References

Barnett MH, Prineas JW (2004) Relapsing and remitting multiple sclerosis: pathology of the newly forming lesion. Ann Neurol 55:458–468.

Bhattacherjee P, Williams RN, Eakins KE (1983) An evaluation of ocular inflammation following the injection of bacterial endotoxin into the rat foot pad. Invest Ophthalmol Vis Sci 24:196–202.

Bitsch A, Schuchardt J, Bunkowski S, Kuhlmann T, Brück W (2000) Acute axonal injury in multiple sclerosis. Correlation with demyelination and inflammation. Brain 123:1174–1183.

Brandt AU, Oberwahrenbrock T, Ringelstein M, Young KL, Tiede M, Hartung HP, Martin R, Aktas O, Paul F, Schippling S (2011) Primary retinal pathology in multiple sclerosis as detected by optical coherence tomography. Brain 134:e193; author reply e194.

De Groot CJ, Bergers E, Kamphorst W, Ravid R, Polman CH, Barkhof F, van der Valk P (2001) Post-mortem MRI-guided sampling of multiple sclerosis brain lesions: increased yield of active demyelinating and (p)reactive lesions. Brain 124:1635–1645.

Diem R, Meyer R, Weishaupt JH, Bähr M (2001) Reduction of potassium currents and phosphatidylinositol 3-kinase-dependent AKT phosphorylation by tumor necrosis factor-α rescues axotomized retinal ganglion cells from retrograde cell death *in vivo*. J Neurosci 21:2058–2066.

Dutta R, Trapp BD (2007) Pathogenesis of axonal and neuronal damage in multiple sclerosis. Neurology 68:S22–S31; discussion S43–S54.

El-Remessy AB, Tang Y, Zhu G, Matragoon S, Khalifa Y, Liu EK, Liu JY, Hanson E, Mian S, Fatteh N, Liou GI (2008) Neuroprotective effects of cannabidiol in endotoxin-induced uveitis: critical role of p38 MAPK activation. Mol Vis 14:2190–2203.

Ferguson B, Matyszak MK, Esiri MM, Perry VH (1997) Axonal damage in acute multiple sclerosis lesions. Brain 120:393–399.

Fisher JB, Jacobs DA, Markowitz CE, Galetta SL, Volpe NJ, Nano-Schiavi ML, Baier ML, Frohman EM, Winslow H, Frohman TC, Calabresi PA, Maguire MG, Cutter GR, Balcer LJ (2006) Relation of visual function to retinal nerve fiber layer thickness in multiple sclerosis. Ophthalmology 113:324–332.

Frischer JM, Bramow S, Dal-Bianco A, Lucchinetti CF, Rauschka H, Schmidbauer M, Laursen H, Sorensen PS, Lassmann H (2009) The relation between inflammation and neurodegeneration in multiple sclerosis brains. Brain 132:1175–1189.

Frohman E, Costello F, Zivadinov R, Stuve O, Conger A, Winslow H, Trip A, Frohman T, Balcer L (2006) Optical coherence tomography in multiple sclerosis. Lancet Neurol 5:853–863.

Gadjanski I, Boretius S, Williams SK, Lingor P, Knöferle J, Sättler MB, Fairless R, Hochmeister S, Sühs KW, Michaelis T, Frahm J, Storch MK, Bähr M, Diem R (2009) Role of N-type voltage-dependent calcium channels in autoimmune optic neuritis. Ann Neurol 66:81–93.

Gay FW, Drye TJ, Dick GW, Esiri MM (1997) The application of multifactorial cluster analysis in the staging of plaques in early multiple sclerosis. Identification and characterization of the primary demyelinating lesion. Brain 120:1461–1483.

Golubnitschaja O, Wunderlich K, Decker C, Mönkemann H, Schild HH, Flammer J (2002) Molecular imaging of perfusion disturbances in glaucoma. Amino Acids 23:293–299.

Gordon-Lipkin E, Chodkowski B, Reich DS, Smith SA, Pulicken M, Balcer LJ, Frohman EM, Cutter G, Calabresi PA (2007) Retinal nerve fiber layer is associated with brain atrophy in multiple sclerosis. Neurology 69:1603–1609.

Green AJ, McQuaid S, Hauser SL, Allen IV, Lyness R (2010) Ocular pathology in multiple sclerosis: retinal atrophy and inflammation irrespective of disease duration. Brain 133:1591–1601.

Grieshaber MC, Flammer J (2007) Does the blood-brain barrier play a role in glaucoma? J Surv Ophthalmol 52 S2:S115–S121.

Henderson AP, Trip SA, Schlottmann PG, Altmann DR, Garway-Heath DF, Plant GT, Miller DH (2008) An investigation of the retinal nerve fibre layer in progressive multiple sclerosis using optical coherence tomography. Brain 131:277–287.

Hobom M, Storch MK, Weissert R, Maier K, Radhakrishnan A, Kramer B, Bähr M, Diem R (2004) Mechanisms and time course of neuronal degeneration in experimental autoimmune encephalomyelitis. Brain Pathol 14:148–157.

Hofbauer A, Dräger UC (1985) Depth segregation of retinal ganglion cells projecting to mouse superior colliculus. J Comp Neurol 234:465–474.

Hu P, Pollard J, Hunt N, Taylor J, Chan-Ling T (1998) Microvascular and cellular responses in the optic nerve of rats with acute experimental allergic encephalomyelitis (EAE). Brain Pathol 8:475–486.

Jha P, Banda H, Tytarenko R, Bora PS, Bora NS (2011) Complement mediated apoptosis leads to the loss to retinal ganglion cells in animal model of glaucoma. Mol Immunol 48:2151–2158.

Kornek B, Storch MK, Weissert R, Wallstroem E, Stefferl A, Olsson T, Linington C, Schmidbauer M, Lassmann H (2000) Multiple sclerosis and chronic autoimmune encephalomyelitis: a comparative quantitative study of axonal injury in active, inactive, and remyelinated lesions. Am J Pathol 157:267–276.

Krishnamoorthy G, Saxena A, Mars LT, Domingues HS, Mentele R, Ben-Nun A, Lassmann H, Dornmair K, Kurschus FC, Liblau RS, Wekerle H (2009) Myelin-specific T cells also recognize neuronal autoantigen in a transgenic mouse model of multiple sclerosis. Nat Med 15:626–632.

Kuhlmann T, Lingfeld G, Bitsch A, Schuchardt J, Brück W (2002) Acute axonal damage in multiple sclerosis is most extensive in early disease and decreases over time. Brain 125:2202–2212.

Langmann T (2007) Microglia activation in retinal degeneration. J Leukoc Biol 81:1345–1351.

Marik C, Felts PA, Bauer J, Lassmann H, Smith KJ (2007) Lesion genesis in a subset of patients with multiple sclerosis: a role for innate immunity? Brain 130:2800–2815.

McMenamin PG, Crewe J (1995) Endotoxin-induced uveitis. Kinetics and phenotype of the inflammatory cell infiltrate and the response of the resident tisue macrophages and dendritic cells in the iris and ciliary body. Invest Ophthalmol Vis Sci 36:1949–1959.

Meyer R, Weissert R, Diem R, Storch MK, de Graaf KL, Kramer B, Bähr M (2001) Acute neuronal apoptosis in a rat model of multiple sclerosis. J Neurosci 21:6214–6220.

Perry VH (1981) Evidence for an amacrine cell system in the ganglion cell layer of the rat retina. Neuroscience 6:931–944.

Perry VH, Cowey A (1979) The effects of unilateral cortical and tectal lesions on retinal ganglion cells in rats. Exp Brain Res 35:85–95.

Perry VH, Morris RJ, Raisman G (1984) Is Thy-1 expressed only by ganglion cells and their axons in the retina and optic nerve? J Neurocytol 13:809–824.

Peterson JW, Bö L, Mörk S, Chang A, Trapp BD (2001) Transected neurites, apoptotic neurons, and reduced inflammation in cortical multiple sclerosis lesions. Ann Neurol 50:389–400.

Portera-Cailliau C, Sung CH, Nathans J, Adler R (1994) Apoptotic photoreceptor cell death in mouse models of retinitis pigmentosa. Proc Natl Acad Sci U S A 91:974–978.

Pulicken M, Gordon-Lipkin E, Balcer LJ, Frohman E, Cutter G, Calabresi PA (2007) Optical coherence tomography and disease subtype in multiple sclerosis. Neurology 69:2085–2092.

Quigley HA (1999) Neuronal death in glaucoma. Prog Retin Eye Res 18:39–57.

Saidha S, Syc SB, Ibrahim MA, Eckstein C, Warner CV, Farrell SK, Oakley JD, Durbin MK, Meyer SA, Balcer LJ, Frohman EM, Rosenzweig JM, Newsome SD, Ratchford JN, Nguyen QD, Calabresi PA (2011) Primary retinal pathology in multiple sclerosis as detected by optical coherence tomography. Brain 134:518–533.

Sättler MB, Togni M, Gadjanski I, Sühs KW, Meyer N, Bähr M, Diem R (2008) Strain-specific susceptibility for neurodegeneration in a rat model of autoimmune optic neuritis. J Neuroimmunol 193:77–86.

Schuetz E, Thanos S (2004) Microglia-targeted pharmocotherapy in retinal neurodegenerative diseases. Curr Drug Targets 5:619–627.

Soto I, Pease ME, Son JL, Shi X, Quigley HA, Marsh-Armstrong N (2011) Retinal ganglion cell loss in a rat ocular hypertension model is sectorial and involves early optic nerve axon loss. Invest Ophthalmol Vis Sci 52:434–441.

Stefferl A, Schubart A, Storch2 M, Amini A, Mather I, Lassmann H, Linington C (2000) Butyrophilin, a milk protein, modulates the encephalitogenic T cell response to myelin oligodendrocyte glycoprotein in experimental autoimmune encephalomyelitis. J Immunol 165:2859–2865.

Stevens B, Allen NJ, Vazquez LE, Howell GR, Christopherson KS, Nouri N, Micheva KD, Mehalow AK, Huberman AD, Stafford B, Sher A, Litke AM, Lambris JD, Smith SJ, John SW, Barres BA (2007) The classical complement cascade mediates CNS synapse elimination. Cell 131:1164–1178.

Storch MK, Stefferl A, Brehm U, Weissert R, Wallström E, Kerschensteiner M, Olsson T, Linington C, Lassmann H (1998) Autoimmunity to myelin oligodendrocyte glycoprotein in rats mimics the spectrum of multiple sclerosis pathology. Brain Pathol 8:681–694.

Trapp BD, Nave KA (2008) Multiple sclerosis: an immune or neurodegenerative disorder? Annu Rev Neurosci 31:247–269.

Trapp BD, Peterson J, Ransohoff RM, Rudick R, Mörk S, Bö L (1998) Axonal transection in the lesions of multiple sclerosis. N Engl J Med 338:278–285.

Traugott U, Stone SH, Raine CS (1978) Experimental allergic encephalomyelitis: migration of early T cells from the circulation into the central nervous system. J Neurol Sci 36:55–61.

Tso MO, Shih CY, McLean IW (1975) Is there a blood-brain barrier at the optic nerve head? Arch Ophthalmol 93:815–825.

Tsuchida M, Hanawa H, Hirahara H, Watanabe H, Matsumoto Y, Sekikawa H, Abo T (1994) Identification of CD4- CD8- alpha beta T cells in the subarachnoid space of rats with experimental autoimmune encephalomyelitis. A possible route by which effector cells invade the lesions. Immunology 81:420–427.

van der Valk P, Amor S (2009) Preactive lesions in multiple sclerosis. Curr Opin Neurol 22:207–213.

Weissert R, Wallström E, Storch MK, Stefferl A, Lorentzen J, Lassmann H, Linington C, Olsson T (1998) MHC haplotype-dependent regulation of MOG-induced EAE in rats. J Clin Invest 102:1265–1273.